JOURNAL OF SOLID STATE CHEMISTRY 114, 516–523 (1995)

Phases in the Perovskite-Type $LaMnO_{3+\delta}$ Solid Solution and the La_2O_3–Mn_2O_3 Phase Diagram

J. A. M. van Roosmalen, P. van Vlaanderen, and E. H. P. Cordfunke

Netherlands Energy Research Foundation ECN, P.O. Box 1, 1755 ZG Petten, The Netherlands

and

W. L. IJdo and D. J. W. IJdo

Gorlaeus Laboratories, Leiden University, P.O. Box 9502, 2300 RA Leiden, The Netherlands

Received July 8, 1993; in revised form May 31, 1994; accepted June 1, 1994

The structural behavior of $LaMnO_{3+\delta}$ is described. One rhombohedral and three different orthorhombic X-ray patterns have been observed. The largest influence on the structure is the overall amount of Mn^{4+}, but the La : Mn ratio and the temperature also have a significant influence. In the pseudobinary La_2O_3–Mn_2O_3 phase diagram, $LaMnO_{3+\delta}$ is the only compound containing both La and Mn. This is not a line compound since a solubility range was observed on both the La-rich and the Mn-rich sides. © 1995 Academic Press, Inc.

1. INTRODUCTION

The structure and the phases of $LaMnO_{3+\delta}$ have been the subject of many investigations (1–19). A number of distorted perovskite-type phases were characterized, but the various results do not form a consistent picture. The oxygen excess in $LaMnO_{3+\delta}$ coincides with the formation of La and Mn vacancies in equal amounts, as was shown by van Roosmalen *et al.* (20, 21) by neutron diffraction, high resolution transmission electron microscopy (HRTEM), and density measurements. For $LaMnO_{3+\delta}$ there is a simple relation between δ and the overall Mn^{4+} content ($Mn^{4+} = 2\delta$)[1]. In (La, Sr)$MnO_{3+\delta}$ and in $LaMnO_{3+\delta}$ with a La : Mn ratio unequal to unity this relation no longer holds. Therefore, instead of δ, the overall Mn^{4+} content is used as a measure of the nonstoichiometry.

The La : Mn ratio is a significant parameter for the performance of $LaMnO_{3+\delta}$ as cathode material in solid oxide fuel cells (SOFCs). If the La : Mn ratio is smaller than unity, the electrical conductivity is increased (24), the sinter curve shifts to lower temperatures (25), and the inertness toward the electrolyte material $Zr_{1-z}Y_zO_{2-\frac{1}{2}z}$ probably increases (26). The polarizability and catalytic activity are probably also affected significantly. To obtain the limits of the perovskite-type $LaMnO_3$ solid solution the pseudobinary La_2O_3–Mn_2O_3 phase diagram has been investigated. The results will be discussed in this article.

2. EXPERIMENTAL

As is discussed elsewhere (25), the diffusion of La is the restricting factor in the formation of $LaMnO_{3+\delta}$. If the influence of the La : Mn ratio is to be studied, this can be a problem. In the La-poor region, where the number of La vacancies and the La diffusion are high, the perovskite-type phase is formed easily. However, in the Mn-poor region the number of La vacancies is small and the perovskite-type phase is formed very slowly. In solid state reaction experiments it is observed that in most cases the perovskite-type phase is formed in the first reaction step, but some of the La_2O_3 does not react. It takes very long firing times at high temperatures, about 100–150 hr at 1300–1400 K, to have the La_2O_3 reacted completely, with four or five intermediate grindings.

Therefore, to prevent the problem of the rather slow reaction of La_2O_3, the coprecipitation method that is described elsewhere (21) was adopted. In this way, La and Mn are mixed intimately on a molecular scale. Moreover,

[1] The defect chemistry of $LaMnO_{3+\delta}$ is rather complicated. Incorporation of oxygen excess in $LaMnO_{3+\delta}$ coincides with the formation of La and Mn vacancies in combination with the partial charge disproportionation of Mn^{3+} into Mn^{2+} and Mn^{4+}, as was shown by van Roosmalen *et al.* (20–23). Omitting the metal-ion vacancies, for simplicity, the defect notation is $LaMn^{2+}_{\xi-2\delta}Mn^{3+}_{1-2\xi+2\delta}Mn^{4+}_{\xi}O_{3+\delta}$, in which ξ is a measure of the charge disproportionation. By wet-chemical redox titration the average Mn valency in excess of 3+ can be found, which is equal to 2δ. Instead of using this complicated description, throughout the article the overall Mn^{4+} content is used as a measure of the oxygen nonstoichiometry. This can be found by considering $LaMn^{3+}_{1-2\delta}Mn^{4+}_{2\delta}O_{3+\delta}$ (overall $Mn^{4+} = 2\delta$), so actually the overall Mn^{4+} content is equal to the average Mn valency in excess of 3+.

0022-4596/95 $6.00
Copyright © 1995 by Academic Press, Inc.
All rights of reproduction in any form reserved.

fine, homogeneous particles, enhancing the reactivity, are thus formed. A disadvantage of the coprecipitation method is that it is difficult to control the La : Mn ratio accurately. Due to the presence of Cl^- and other ions during the washing of the precipitated powder, the La : Mn ratio might change, although only slightly (not more than 1% in our experiments).

It is hard to analyze both the La and the Mn content in the same sample by wet-chemical methods. The accuracy of inductively coupled plasma emission spectroscopy (ICP) is about 1%. To investigate the relationship between the La : Mn ratio and the lattice parameters, coprecipitated powders prepared in rather large amounts (about 40 g), were used. This resulted in three powders with compositions La : Mn of 0.91, 1.00, and 1.03, ± 0.01. Samples with different contents of Mn^{4+} were obtained by firing under oxygen, air, or argon atmospheres at temperatures between 1070 and 1480 K in platinum crucibles. The overall Mn^{4+} content was determined by standard wet-chemical redox titrations, using MnO_4^- and Fe^{2+}.

To investigate the La_2O_3–Mn_2O_3 phase diagram, the La : Mn ratio must be known more accurately. For this reason a combination of precipitation and solid state reaction was chosen. La and Mn were precipitated separately, in the same way as that described elsewhere (21). The precipitates were dried at 373 K and annealed at 873 K. In this way small, reactive particles were formed. For each of the precipitates an accurate wet-chemical analysis was made. The chemical analysis and the X-ray pattern of the annealed Mn precipitate indicated Mn_2O_3, while the La precipitate appeared to be $La_2O_2CO_3$. To obtain various compositions the La and Mn precipitates were weighed in the appropriate amounts and mixed thoroughly in an argon-filled glove box. The reaction was much faster than the original solid state reaction between La_2O_3 and Mn_2O_3. Nevertheless, at the La-rich boundary of the $LaMnO_3$ solid solution range, long reaction times (up to 100 hr) and intermediate grindings were necessary at low reaction temperatures (1123 and 1273 K).

Room temperature lattice constants were determined using Cu$K\alpha_1$ radiation with an internal standard of W (a_0 = 0.316540 nm) and Si (a_0 = 0.543083 nm). High-temperature measurements were performed from room temperature up to 1373 K with a Guinier–Lenné camera, using a platinum grid. Heat effects were measured using a Mettler TA-13 differential scanning calorimetry (DSC) apparatus.

3. PHASES IN THE PEROVSKITE-TYPE $LaMnO_{3+\delta}$ SOLID SOLUTION

The oxygen content of $LaMnO_{3+\delta}$ is a function of temperature and oxygen partial pressure at high temperatures. Below about 900 K, however, the exchange of oxygen with the surrounding gas atmosphere is so slow that the effect on δ is negligible. In strong reducing atmospheres oxygen can be removed from the lattice at lower temperatures (16). By choosing the right temperatures and oxygen partial pressures and cooling rapidly after equilibration, a wide range of oxygen contents can be obtained at room temperature.

$LaMnO_{3+\delta}$ can crystallize with either orthorhombic or rhombohedral symmetry, depending on the value of δ. $LaMnO_{3.0}$ crystallizes with orthorhombic symmetry, space group *Pnma* with $Z = 4$ (Z is the number of formula units in the unit cell), as was determined by neutron powder diffraction by Elemans *et al.* (10). $LaMnO_{3.0}$ is isostructural with $GdFeO_3$ (27). At high values of δ, La $MnO_{3+\delta}$ crystallizes with rhombohedral symmetry, space group $R\bar{3}c$ with $Z = 2$. This was shown by Tofield and Scott (11) using neutron powder diffraction on a sample with composition $LaMnO_{3.12}$, and was recently confirmed by van Roosmalen *et al.* (20) for a sample with composition $LaMnO_{3.158}$.

First, to examine the relationship between the lattice parameters and δ, a comparison of the available data has been made. It is most convenient to use the unit cell volumes. All results obtained by various authors (1–19), including the present results, are plotted in Fig. 1a, with $Z = 4$. Differences in the data obtained by various authors are most likely to be caused by differences in the La : Mn ratio (all data represent an assumed ratio of La : Mn = 1 : 1), or by difficulties in wet-chemical analysis, rather than by the unit cell volume determination itself. The closed circles in Fig. 1a represent samples with a La : Mn ratio close to 1 : 1. Bogush *et al.* (17) found a two-phase region at intermediate values of δ. All other data, including the present results, indicate a single phase region. This seems to be a crystallization or interpretation problem rather than a difference in La : Mn ratio. For this reason only the results of Bogush *et al.* (17) in the intermediate range are excluded. The data representing a La : Mn ratio of 1 : 1 are shown again in Fig. 1b, to show the contributions of the various authors.

The unit cell volumes representing a La : Mn ratio of 1 : 1, can be fitted linearly or with a third-order polynomial. The linear fit is expressed as

$$V = (244.86 - 68.81 \cdot \delta) \times 10^{-24}\ \text{cm}^3. \quad [1]$$

The polynomial fit is expressed as

$$V = (244.55 - 24.97 \cdot \delta - 850.0 \cdot \delta^2 + 3918 \cdot \delta^3) \times 10^{-24}\ \text{cm}^3. \quad [2]$$

In Fig. 1a the polynomial fit is used to clarify the relationship between the unit cell volume and the Mn^{4+} content

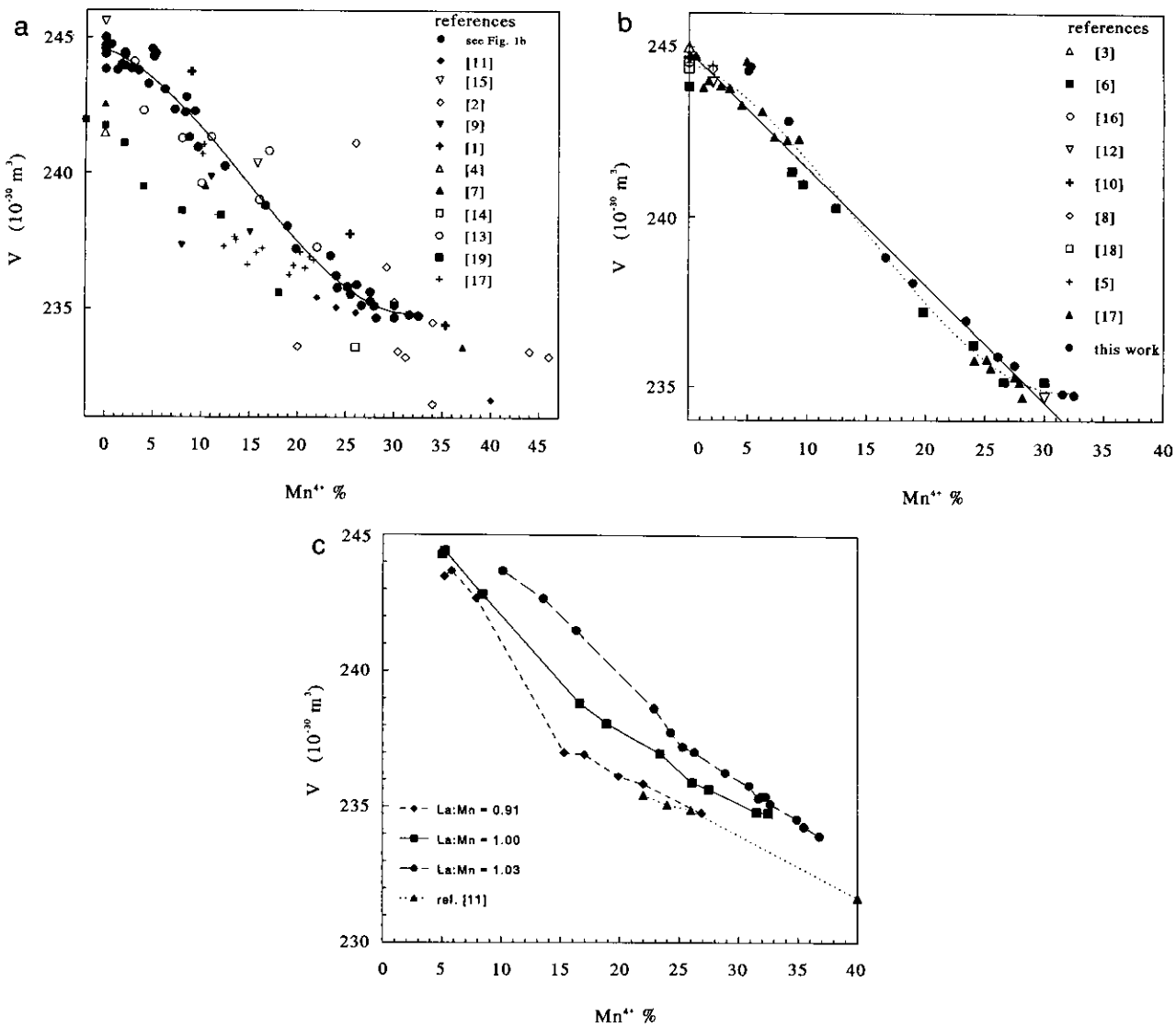

FIG. 1. Unit cell volumes as a function of the overall amount of Mn^{4+} (represented as percentage of the total amount of Mn): (a) results from literature on $LaMnO_{3+\delta}$ (with La : Mn = 1) including the present work. The results that show good agreement are represented as closed circles and are fitted to the drawn line (third-order polynomial fit); (b) the results from Fig. 1a that show good agreement, fitted linearly and to a third-order polynomial; (c) present results on $LaMnO_{3+\delta}$ with various La : Mn ratios. The results of Tofield and Scott (11) are added to indicate that probably their La : Mn ratio was smaller than unity.

for the data where La : Mn = 1 : 1. For practical purposes it is more convenient to use the linear fit (Fig. 1b), for instance, to calculate the density of $LaMnO_{3+\delta}$ as a function of δ (21).

In Fig. 1c the results obtained in the present study on $LaMnO_{3+\delta}$ with various La : Mn ratios are shown, together with the results of Tofield and Scott (11). It is obvious that the relationship between unit cell volume and the overall Mn^{4+} content is strongly influenced by the La : Mn ratio. The results of Tofield and Scott (11) indicate that the La : Mn ratio of their samples was less than unity, although they assumed themselves that it was unity. Unfortunately, no chemical analyses on the La : Mn ratio of their data are available.

In the discussion of the defect chemistry of $LaMnO_{3+\delta}$ ($= La_{1-\gamma}Mn_{1-\gamma}O_3$) (20–22) the ratio of La : Mn vacancies is very important. Tofield and Scott (11) found more lanthanum than manganese vacancies by neutron diffraction, which can be understood if indeed the La : Mn ratio of their sample was smaller than unity (Fig. 1c). Van Roosmalen *et al.* (20) found an equal number of lanthanum and manganese vacancies in a sample with a La : Mn ratio of 1.00 + 0.01 by neutron diffraction. On the basis of these results van Roosmalen and Cordfunke (22) suggested a

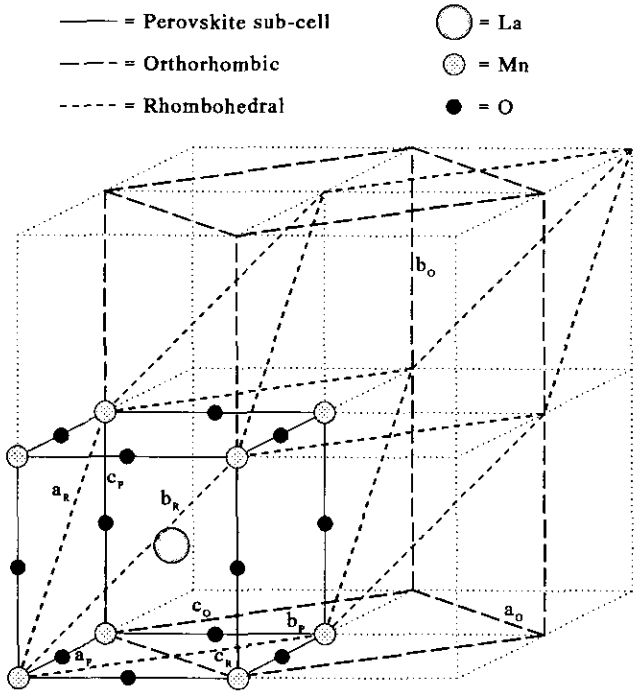

FIG. 2. Comparison of the orthorhombic and rhombohedral unit cell of $LaMnO_{3+\delta}$, drawn in a nondistorted perovskite structure. Both can be expressed in the perovskite subcell.

defect model that describes the defect chemistry of La $MnO_{3+\delta}$ satisfactorily.

Now a closer examination can be made of the phases in the perovskite-type $LaMnO_{3+\delta}$ solid solution on the basis of the lattice parameters. To compare the results obtained on orthorhombic and rhombohedral $LaMnO_{3+\delta}$, all lattice parameters are expressed in the perovskite subcell ($Z = 1$), as shown in Fig. 2. In this figure the ideal perovskite structure is drawn with atoms only in the perovskite subcell; a_P, b_P, c_P, α_P, β_P, and γ_P are used to describe the phases of $LaMnO_{3+\delta}$.

Guinier–de Wolff recordings of $LaMnO_{3+\delta}$ samples with various compositions (both orthorhombic and rhombohedral) show some weak reflections that cannot be described in the usual unit cell, but can be described in a cell with doubled axes. Van Roosmalen *et al.* (20) have shown by neutron diffraction that doubling of the unit cell is likely for rhombohedral $LaMnO_{3+\delta}$. This was also observed by Tofield and Scott (11), and for orthorhombic $LaMnO_{3.00}$ by Elemans *et al.* (10). Neutron diffraction results (20) indicate that the atomic positions in the doubled unit cell are shifted only slightly and that the structure of the $LaMnO_{3+\delta}$ samples can be described satisfactorily in the usual orthorhombic and rhombohedral unit cells (Fig. 2).

The lattice parameters of the various samples that were synthesized are listed in Table 1 together with their transformation to the perovskite subcell. In Fig. 3 the (subcell) results are shown. Four different types of Guinier–de Wolff patterns were observed. They coincide with four different relations between the subcell lattice parameters:

1. $a_P = b_P > c_P, \gamma_P > \alpha_P = \beta_P = 90°$
2. $a_P = b_P > c_P, \gamma_P < \alpha_P = \beta_P = 90°$
3. $a_P = b_P < c_P, \gamma_P < \alpha_P = \beta_P = 90°$
4. $a_P = b_P = c_P, \gamma_P = \alpha_P = \beta_P < 90°$.

Patterns 1, 2, and 3 correspond to an orthorhombic symmetry that is the result of tilting of the MnO_6 octahedra in the perovskite-type structure.

From the present results it is not clear whether the three patterns are the result of the same sort of tilts with different magnitudes, or from different sorts of tilts. The latter case would correspond to three different orthorhombic phases. The first pattern corresponds to the orthorhombic structure as was determined for $LaMnO_{3.0}$ by Elemans *et al.* (10), with space group *Pnma*. The second pattern was also identified by Takeda *et al.* (19). The third pattern only occurs if La : Mn > 1 and has not yet been reported. Pattern 4 corresponds to the rhombohedral structure with space group $R\bar{3}c$ that was determined for $LaMnO_{3.12}$ and $LaMnO_{3.158}$ by Tofield and Scott (11), and by van Roosmalen *et al.* (20), respectively. For $LaMnO_{3+\delta}$ (with La : Mn = 1) the transition from pattern 1 to pattern 2 is at about 16% Mn^{4+}. The orthorhombic to rhombohedral phase transformation occurs at about 25% Mn^{4+}.

Apparently, the structural behavior of $LaMnO_{3+\delta}$ is very complicated. The number of patterns that is found increases with an increase in the La : Mn ratio. For La : Mn = 0.91, patterns 1 and 4 have been found (although it cannot be excluded that pattern 2 can be found for samples with compositions between pattern 1 and pattern 4). Patterns 1, 2, and 4 have been found for La : Mn = 1.00, while for La : Mn = 1.03 all four patterns have been observed. The largest influence on the structure of $LaMnO_{3+\delta}$, however, is the overall amount of Mn^{4+}. The cooperative ordering of the Jahn–Teller distorted $Mn^{3+}O_6$ octahedra leads to the orthorhombic structure of $LaMnO_{3.0}$. This ordering is destroyed by an increase in the overall amount of Mn^{4+}, which is the major influence on the room temperature structure of $LaMnO_{3+\delta}$. This is due to an increase in the oxygen content. In $La_{1-x}Sr_xMnO_{3+\delta}$ it is known that with an increasing amount of strontium (x), the overall amount of Mn^{4+} also increases, destroying the ordering, as was already shown by Jonker (3). Recently, this has also been reported for $Pr_{1-x}Sr_xMnO_3$ (28).

Wold and Arnott (6) have shown that ordering of the Jahn–Teller octahedra can also be destroyed by tempera-

TABLE 1

Lattice Parameters (in 10^{-1} nm) for $LaMnO_{3+\delta}$ with Various La : Mn Ratios, Estimated Standard Deviations in Parentheses (The Unit Cell Volume (V) Is Given for Four Formula Units, Corresponding to the Orthorhombic Unit Cell)

La : Mn	Mn^{4+}%	a	b	c	α_R	$a_p = b_p$	c_p	γ_p	V
0.91	5.2	5.5295(9)	7.7137(10)	5.7081(6)	—	3.9736	3.8569	91.821	243.47
	5.8	5.5333(6)	7.7126(13)	5.7101(11)	—	3.9756	3.8563	91.802	243.68
	7.9	5.5274(17)	7.7111(12)	5.6938(18)	—	3.9677	3.8556	91.699	242.68
	15.3	5.4856(2)	5.4856(2)	5.4856(2)	60.675(2)	3.8987	3.8987	89.419	237.00
	17.0	5.4790(1)	5.4790(1)	5.4790(1)	60.666(1)	3.8982	3.8982	89.427	236.92
	19.9	5.4807(2)	5.4807(2)	5.4807(2)	60.625(3)	3.8938	3.8938	89.462	236.12
	22.0	5.4792(2)	5.4792(2)	5.4792(2)	60.611(2)	3.8923	3.8923	89.474	235.84
	26.9	5.4730(1)	5.4730(1)	5.4730(1)	60.557(1)	3.8863	3.8863	89.520	234.76
1.00	5.0	5.5343(5)	7.7010(10)	5.7317(12)	—	3.9838	3.8505	92.007	244.29
	5.2	5.5320(4)	7.7010(12)	5.7373(13)	—	3.9850	3.8505	92.087	244.42
	8.4	5.5316(4)	7.7154(12)	5.6896(56)	—	3.9677	3.8577	91.613	242.81
	16.6	5.5396(20)	7.7897(27)	5.5340(42)	—	3.9151	3.8949	89.942	238.81
	18.9	5.5402(5)	7.7978(10)	5.5107(12)	—	3.9071	3.8989	89.694	238.06
	23.4	5.5394(7)	7.7838(12)	5.4957(7)	—	3.9015	3.8919	89.546	236.96
	26.1	5.5339(3)	7.7850(7)	5.4757(3)	—	3.8925	3.8925	89.394	235.90
	27.5	5.4740(3)	5.4740(3)	5.4740(3)	60.705(4)	3.8914	3.8914	89.394	235.64
	31.5	5.4716(1)	5.4716(1)	5.4716(1)	60.675(1)	3.8866	3.8866	89.419	234.80
	32.5	5.4696(2)	5.4696(2)	5.4696(2)	60.638(2)	3.8863	3.8863	89.451	234.76
1.03	10.1	5.5342(3)	7.7039(5)	5.7156(6)	—	3.9779	3.8520	91.848	243.68
	13.5	5.5357(5)	7.7144(5)	5.6826(12)	—	3.9666	3.8572	91.500	242.67
	16.3	5.5269(17)	7.7266(12)	5.6549(14)	—	3.9536	3.8633	91.312	241.49
	22.9	5.5393(6)	7.7858(10)	5.5331(5)	—	3.9147	3.8929	89.936	238.63
	24.3	5.5398(8)	7.7878(12)	5.5109(9)	—	3.9070	3.8939	89.700	237.75
	25.3	5.5377(11)	7.7916(19)	5.4976(12)	—	3.9016	3.8958	89.584	237.21
	26.3	5.5377(13)	7.7894(17)	5.4948(13)	—	3.9006	3.8947	89.554	237.02
	28.9	5.5376(4)	7.7921(6)	5.4754(2)	—	3.8937	3.8961	89.352	236.26
	30.9	5.5291(25)	7.7882(17)	5.4755(7)	—	3.8908	3.8941	89.442	235.78
	31.7	5.4731(3)	5.4731(3)	5.4731(3)	60.667(4)	3.8896	3.8896	89.426	235.30
	31.9	5.4736(2)	5.4736(2)	5.4736(2)	60.654(3)	3.8896	3.8896	89.437	235.37
	32.3	5.4731(3)	5.4731(3)	5.4731(3)	60.678(3)	3.8899	3.8899	89.417	235.38
	32.7	5.4717(2)	5.4717(2)	5.4717(2)	60.663(2)	3.8885	3.8885	89.430	235.10
	34.9	5.4686(2)	5.4686(2)	5.4686(2)	60.627(3)	3.8852	3.8852	89.460	234.54
	35.5	5.4669(4)	5.4669(4)	5.4669(4)	60.619(4)	3.8838	3.8838	89.467	234.26
	36.8	5.4635(2)	5.4635(2)	5.4635(2)	60.630(2)	3.8817	3.8817	89.458	233.92

ture. The lattice parameters of $LaMnO_{3+\delta}$ show the same behavior with an increase in temperature as does the room temperature structure as a function of Mn^{4+} content. In other words, $LaMnO_{3+\delta}$ (with La : Mn = 1) in pattern 1 at room temperature will transform to pattern 2 and pattern 4 if the temperature is raised.

This is shown in the high-temperature Guinier–Lenné recording in air (Fig. 4) on a sample with an overall Mn^{4+} content of 3.6%. At 650 ± 30 K pattern 1 transforms into pattern 2. The transformation from pattern 2 to pattern 4 occurs at 870 ± 30 K. Around 960 ± 30 K the lattice parameters of pattern 4 change significantly. This is due to the uptake of oxygen by the lattice and a subsequent increase of the overall Mn^{4+} content. Thermal gravimetric analyses (TGA) show that the uptake of oxygen by the lattice below this temperature, under the high-temperature Guinier–Lenné recording conditions and DSC conditions (see below) is negligible. At around 1000 K the equilibrium oxygen content of $LaMnO_{3+\delta}$ in air corresponds with a Mn^{4+} content on the order of 30% (22).

An indication of the possibility that all four patterns correspond to different phases has been obtained by DSC. The transition from pattern 1 to pattern 2 (Fig. 4) at 650 ± 30 K is rather abrupt. The heat effect that is associated with this transition is determined to be 1.1 ± 0.2 kJ · $mole^{-1}$ at 650 ± 5 K using DSC. This might indicate that a phase transformation is involved. However, a sudden change in the tilt of the MnO_6 octahedra without a phase transformation could also give rise to such a heat effect. It was also observed that the heat effect depends on the Mn^{4+} content. A sample with 9.8% Mn^{4+}, for instance, showed no heat effect, nor an abrupt change in lattice parameters at the transition from pattern 1 to 2. Conductivity measurements (24) also indicate that the magnitude

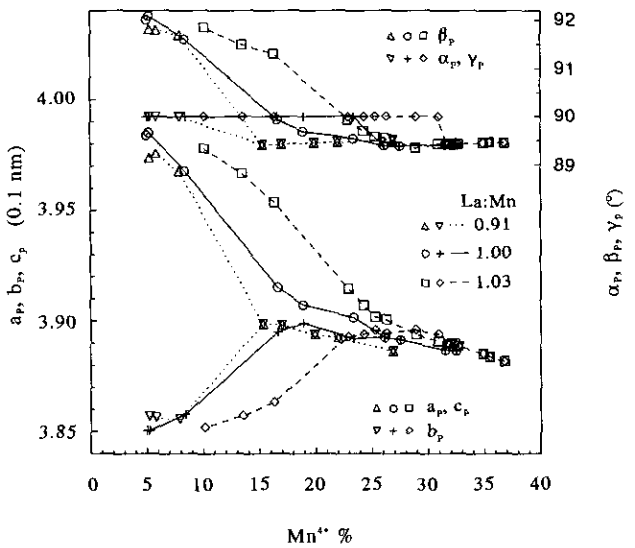

FIG. 3. Lattice parameters of $LaMnO_{3+\delta}$ with various La : Mn ratios expressed in the perovskite subcell. Cell axes are expressed on the left y-axis, angles on the right y-axis. The lattice parameters correspond with two X-ray patterns for La : Mn = 0.91, three for La : Mn = 1.00, and four for La : Mn = 1.03.

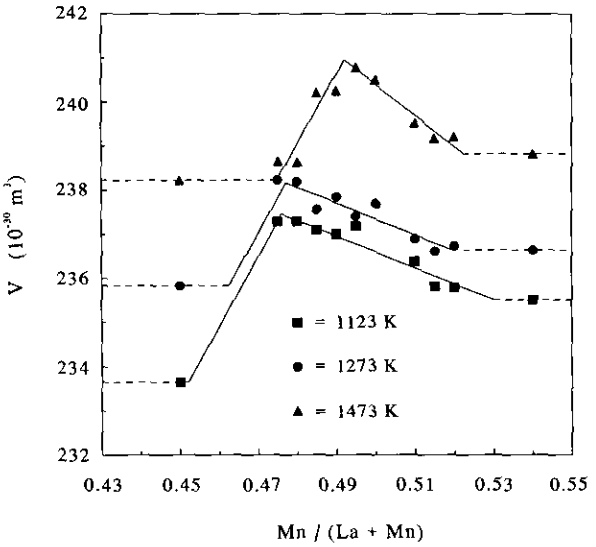

FIG. 5. Unit cell volumes of the $LaMnO_{3+\delta}$ solid solution phase as a function of the Mn : La + Mn ratio quenched from 1123, 1273, and 1473 K.

of the change in lattice parameters (and the associated heat effect) decreases with increasing Mn^{4+} content.

A transition that involves a change in the tilt of the octahedra as well as a phase transformation is the orthorhombic to rhombohedral phase transformation. For $LaMnO_{3+\delta}$ (La : Mn = 1 : 1) the room temperature structure changes from orthorhombic (pattern 2) to rhombohedral (pattern 4) at about 25% of Mn^{4+}. At this transition the (sub) cell axes shade off into one another, but the cell angles α_P and β_P change abruptly (Fig. 3). The heat effect that was measured by DSC for this transformation on a sample with 9.8% of Mn^{4+} is 410 ± 40 $J \cdot mole^{-1}$ at 807 ± 1 K. This is in good agreement with the results obtained by Momin *et al.* (29) on the orthorhombic to rhombohedral phase transition in $LaCrO_3$.

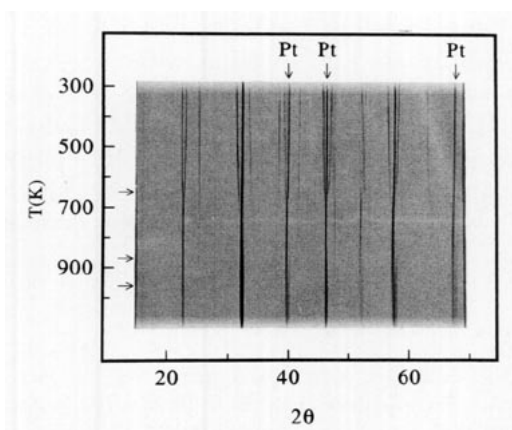

FIG. 4. Guinier–Lenné recording on $LaMnO_{3.018}$ from room temperature to 1030 K in air. At 650 ± 30 K pattern 1 (see text) transforms into pattern 2, which transforms to pattern 4 at 870 ± 30 K. Around 960 ± 30 K the sample takes up oxygen. Pattern 4 remains, but the lattice parameters change significantly.

4. THE La_2O_3–Mn_2O_3 PHASE DIAGRAM

The most interesting part of the La_2O_3–Mn_2O_3 phase diagram for applications in SOFC is the $LaMnO_3$ perovskite-type solid solution. To determine the solid solution region the unit cell volumes were determined for a number of samples in and out of the region, equilibrated at 1123, 1273, and 1473 K in air. After equilibration the samples were quenched to room temperature. The results are shown in Fig. 5. The Mn-rich side could be determined reasonably well. It appears that at the three different temperatures the boundary is more or less the same. It is suggested that the Mn-rich boundary is independent of temperature, at least to 1970 K (see Fig. 6). The average of the boundaries as determined from the unit cell volumes becomes Mn/(La + Mn) = 0.524. This is in good agreement with the results obtained by Takeda *et al.* (19).

The La-rich boundary could only be established well at 1473 K, the boundary lies at Mn/(La + Mn) = 0.475. As was mentioned under Experimental, at 1123 and 1273 K the reaction between the starting products proceeds slowly. The behavior at 1123 and 1273 K on the Mn-rich side is different from that at 1473 K. It is assumed, however, that the behavior at the La-rich side is the same at 1123, 1273, and 1473 K. An indication for this is the

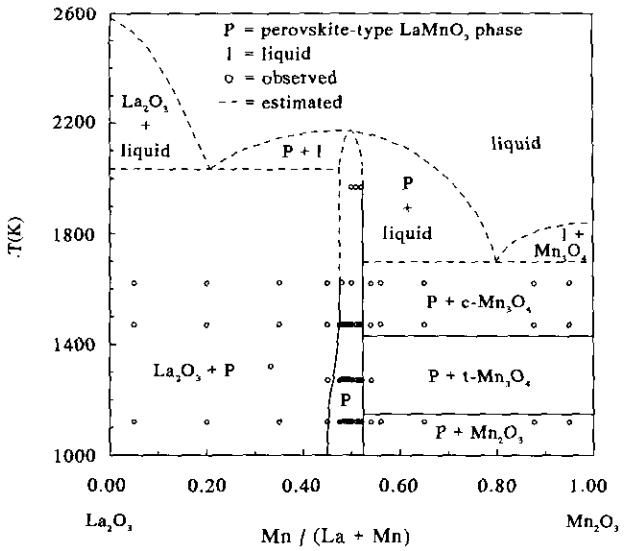

FIG. 6. The pseudobinary La_2O_3–Mn_2O_3 phase diagram in air. Mn_2O_3 loses oxygen at the transformation to Mn_3O_4.

sample where Mn/(La + Mn) = 0.45 at 1123 K. This sample was given enough time to equilibrate, and it was found to contain a small amount of La_2O_3 in addition to the $LaMnO_3$ perovskite-type phase. Using the slope that was found for the 1473 K results, the boundaries at 1123 and 1273 K are calculated to be 0.452 and 0.462, respectively.

The range in which the $LaMnO_3$ perovskite-type phase can occur at 1123 K in air is between $La_{0.908}MnO_3$ and $La_{1.202}MnO_3$ (in the correct defect notation this should be written as $LaMn_{0.832}O_3$). At lower temperatures or higher oxygen partial pressures the range might be a little larger, but probably not significantly. Above about 1400 K, almost to the melting point of $LaMnO_3$, the solid solution range becomes more symmetrical with boundaries at about $La_{0.91}MnO_3$ and $La_{1.10}MnO_3$. $LaMnO_3$ is one of the few known perovskite-type compounds to show such a large range of metal ion vacancies on both the *A*(La) site and the *B*(Mn) site.

The pseudobinary La_2O_3/Mn_2O_3 phase diagram in air is shown in Fig. 6. Apart from the perovskite-type $LaMnO_3$ solid solution no other phases containing La as well as Mn were found in samples with composition Mn/(La + Mn) = 0.050, 0.200, 0.350, 0.450, 0.540, 0.560, 0.650, 0.877, and 0.950 at 1123, 1473, and 1623 K and a sample with Mn/(La + Mn) = 0.333 at 1323 K. No melting phenomena were observed in samples with composition Mn/(La + Mn) = 0.500, 0.510, and 0.520 at 1970 K. The melting point of 2173 K for $LaMnO_3$ was reported by King *et al.* (30). The Mn_2O_3 to tetragonal Mn_3O_4 phase transformation with oxygen loss at 1150 K, the tetragonal Mn_3O_4 to cubic Mn_3O_4 phase transformation at 1433 ± 5 K, and the melting point of cubic Mn_3O_4 at 1840 ± 5 K were reported by Ranganathan *et al.* (31). The melting point of La_2O_3 was assessed by Cordfunke and Konings (32) and found to be 2582 ± 9 K. The estimated part of the phase diagram is based on the La_2O_3–Fe_2O_3 phase diagram, reported by Moruzzi and Shafer (33). Fe_2O_3 transforms to Fe_3O_4, similar to Mn_2O_3, and Fe_3O_4 melts at 1864 K (33). The melting point of $LaFeO_3$ is 2163 ± 30 K (33).

5. CONCLUSIONS

For practical purposes, the relation between the unit cell volumes and the Mn^{4+} content in $LaMnO_{3+\delta}$ can be fitted to a straight line. However, the structural behavior of $LaMnO_{3+\delta}$ is not straightforward. With increasing Mn^{4+} content the unit cell volume decreases and the symmetry changes. With a low Mn^{4+} content an orthorhombic symmetry with a rather large deviation from the ideal perovskite structure has been found. This is due to ordering of the Jahn-Teller distorted $Mn^{3+}O_6$ octahedra. The ordering is destroyed by an increase in the Mn^{4+} content, resulting in a rhombohedral symmetry for a high Mn^{4+} content.

With an intermediate Mn^{4+} content the behavior is complicated and depends on the La : Mn ratio. With La : Mn = 0.91 the orthorhombic structure mentioned above (pattern 1) is followed directly by the rhombohedral structure (pattern 4). For La : Mn = 1.00, however, an additional orthorhombic Guinier–de Wolff pattern has been observed (pattern 2). With a low Mn^{4+} content pattern 1 is formed, with an intermediate Mn^{4+} content pattern 2 is observed, and pattern 4 is found for a high Mn^{4+} content. For La : Mn = 1.03 a third orthorhombic pattern is observed (pattern 3), that is formed with a Mn^{4+} content intermediate between that of patterns 2 and 4.

From the La_2O_3–Mn_2O_3 phase diagram it can be seen that the perovskite-type $LaMnO_{3+\delta}$ solid solution can be formed with excess La as well as with excess Mn. The range in which the $LaMnO_3$ perovskite-type phase can occur at 1123 K in air is between a La : Mn ratio of 0.908 and 1.202. At temperatures above 1400 K, almost to the melting point of $LaMnO_3$, the range becomes more symmetrical, with boundaries at La : Mn ratios of about 0.91 and 1.10.

ACKNOWLEDGMENTS

The authors thank Mrs. A. Scheele for performing the DSC measurements and Mr. P. C. Konijn and Mr. B. C. Broersen for performing the chemical analyses.

REFERENCES

1. H. L. Yakel, Jr., *Acta Crystallogr.* **8**, 394 (1955).
2. M. G. Harwood, *Proc. Phys. Soc. London, Sect. B* **68**, 586 (1955).

3. G. H. Jonker, *Physica* **22,** 707 (1956).
4. M. A. Gilleo, *Acta Crystallogr.* **10,** 161 (1957).
5. U. H. Bents, *Phys. Rev.* **106,** 225 (1957).
6. A. Wold and R. J. Arnott, *J. Phys. Chem. Solids* **9,** 176 (1959).
7. H. Watanabe, *J. Phys. Soc. Jpn.* **16,** 433 (1961).
8. G. H. Jonker, *J. Appl. Phys.* **37,** 1424 (1966).
9. C. M. Iserentant, *Verh. K. Vlaam. Acad. Wet., Lett. Schone Kunsten Belg. Kl. Wet.* **30,** 1 (1968).
10. J. B. A. A. Elemans, B. van Laar, K. R. van der Veen, and B. O. Loopstra, *J. Solid State Chem.* **3,** 238 (1971).
11. B. C. Tofield and W. R. Scott, *J. Solid State Chem.* **10,** 183 (1974).
12. R. J. H. Voorhoeve, J. P. Remeika, L. E. Trimble, A. S. Cooper, F. J. Disalvo, and P. K. Gallagher, *J. Solid State Chem.* **14,** 395 (1975).
13. N. N. Sirota, A. P. Karavay, and V. I. Pavlov, *Krist. Tech.* **11,** 861 (1976).
14. P. K. Gallagher, D. W. Johnson, Jr., and E. M. Vogel, *J. Am. Ceram. Soc.* **60,** 28 (1977).
15. K. Kamata, T. Nakajima, T. Hayashi, and T. Nakamura, *Mater. Res. Bull.* **13,** 49 (1978).
16. F. Abbattista and M. Lucco Borlera, *Ceram. Int.* **7,** 137 (1981).
17. A. K. Bogush, V. I. Pavlov, and L. V. Balyko, *Cryst. Res. Technol.* **18,** 589 (1983).
18. T. Hashimoto, N. Ishizawa, N. Mizutani, and M. Kato, *J. Cryst. Growth* **84,** 207 (1987).
19. Y. Takeda, S. Nakai, T. Kojima, R. Kanno, N. Imanishi, G. Q. Shen, O. Yamamoto, M. Mori, C. Asakawa, and T. Abe, *Mater. Res. Bull.* **26,** 153 (1991).
20. J. A. M. van Roosmalen, E. H. P. Cordfunke, R. B. Helmholdt, and H. W. Zandbergen, *J. Solid State Chem.* **110,** 100 (1994).
21. J. A. M. van Roosmalen and E. H. P. Cordfunke, *J. Solid State Chem.* **110,** 106 (1994).
22. J. A. M. van Roosmalen and E. H. P. Cordfunke, *J. Solid State Chem.* **110,** 109 (1994).
23. J. A. M. van Roosmalen and E. H. P. Cordfunke, *J. Solid State Chem.* **110,** 113 (1994).
24. J. A. M. van Roosmalen, J. P. P. Huijsmans, and L. Plomp, *Solid State Ionics* **66,** 279 (1994).
25. J. A. M. van Roosmalen, E. H. P. Cordfunke, and J. P. P. Huijsmans, *Solid State Ionics* **66,** 285 (1994).
26. J. A. M. van Roosmalen and E. H. P. Cordfunke, *Solid State Ionics* **52,** 303 (1992).
27. S. Geller, *J. Chem. Phys.* **24,** 1236 (1956).
28. K. Knížek, Z. Jirák, E. Pollert, T. Zounová, and S. Vratislav, *J. Solid State Chem.* **100,** 292 (1992).
29. A. C. Momin, E. B. Mirza, and M. D. Mathews, *J. Mater. Sci. Lett.* **10,** 1246 (1991).
30. H. W. King, K. M. Castelliz, G. J. Murphy, and W. Manuel, *J. Can. Ceram. Soc.* **51,** 1 (1982).
31. T. Ranganathan, B. E. MacKean, and A. Muan, *J. Am. Ceram. Soc.* **45,** 279 (1962).
32. E. H. P. Cordfunke and R. J. M. Konings (Eds.), "Thermochemical Data for Reactor Materials and Fission Products." North-Holland, Amsterdam 1990.
33. V. L. Moruzzi and M. W. Shafer, *J. Am. Ceram. Soc.* **43,** 367 (1960).